An Ultrasensitive Electrochemiluminescence Biosensor for Detection of MicroRNA by in-situ Electrochemically Generated Copper Nanoclusters as Luminophore and TiO_2 as Coreaction Accelerator

Hongxia Liao, Ying Zhou, Yaqin Chai, Ruo Yuan

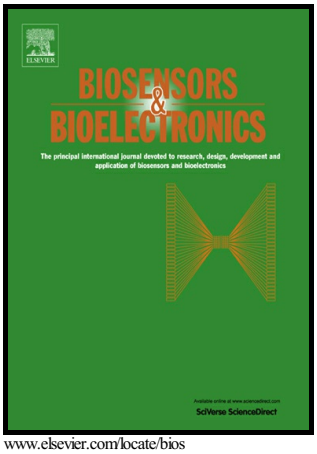

www.elsevier.com/locate/bios

PII: S0956-5663(18)30350-6
DOI: https://doi.org/10.1016/j.bios.2018.05.011
Reference: BIOS10469

To appear in: *Biosensors and Bioelectronic*

Received date: 6 February 2018
Revised date: 27 April 2018
Accepted date: 7 May 2018

Cite this article as: Hongxia Liao, Ying Zhou, Yaqin Chai and Ruo Yuan, An Ultrasensitive Electrochemiluminescence Biosensor for Detection of MicroRNA by in-situ Electrochemically Generated Copper Nanoclusters as Luminophore and TiO_2 as Coreaction Accelerator, *Biosensors and Bioelectronic,* https://doi.org/10.1016/j.bios.2018.05.011

An Ultrasensitive Electrochemiluminescence Biosensor for Detection of MicroRNA by in-situ Electrochemically Generated Copper Nanoclusters as Luminophore and TiO_2 as Coreaction Accelerator

Hongxia Liao, Ying Zhou, Yaqin Chai*, Ruo Yuan*

Key Laboratory of Luminescent and Real-Time Analytical Chemistry (Southwest University), Ministry of Education, College of Chemistry and Chemial Engineering, Southwest University, Chongqing 400715, China

*Corresponding authors at: Tel.: +86 23 68252277; fax: +86 23 68253172
yqchai@swu.edu.cn
yuanruo@swu.edu.cn

ABSTRACT

Herin, we constructed an ultrasensitive electrochemiluminescence (ECL) biosensor for detecting microRNA-21 (miR-21) based on in-situ generation of copper nanoclusters (Cu NCs) as luminophore and titanium dioxide (TiO_2) as coreaction accelerator. First, numerous AT-rich double-stranded DNA (dsDNA) was produced from the conversion of a small amount of target miR-21 *via* the combination of exonuclease III (Exo III)-assisted amplification and hybridization chain reaction (HCR), which could reduce the aggregation-caused self-etching effect of Cu NCs and improve the emitting of Cu NCs. Simultaneously, the introduction of TiO_2 in the sensing interface not just acted as the immobilizer of dsDNA-stabilized Cu NCs, more than acted as the coreaction accelerator to accelerate the reduction of the coreaction reagent ($S_2O_8^{2-}$) for significantly enhancing the ECL efficiency of Cu NCs. The

biosensor showed an excellent linear relationship in the concentration range from 100 aM to 100 pM with the detection limit of 19.05 aM. Impressively, the strategy not only opened up a novel and efficient preparation method for the Cu NCs, but expanded the application of Cu NCs in ultrasensitive biodetection owing to the addition of coreaction accelerator.

Keywords: microRNA-21 (miR-21); Cu nanoclusters (Cu NCs); titanium dioxide (TiO_2); in-situ electrochemical generation

1. Introduction

It was known to all that breast cancer has become a serious threat to the health of women, with progressively increased incidence and mortality. microRNA-21 (miR-21), a noncoding single-stranded RNA molecule with a length of about 22 nucleotides, had been identified as a potential biomarker for the progression and prognosis diagnosis of breast cancer (Zaleska et al., 2017). Therefore, the ultrasensitive detection of miR-21 has been widely concerned by researchers. At present, various methods for miR-21 detection were reported, including fluorescence, photoelectrochemistry, electrochemistry and electrochemiluminescence (ECL) (Lu et al., 2017; Wu et al., 2016; Chen et al., 2016). ECL was one of the most prospective analysis methods to meet the needs of miR-21 detection owing to the high sensitivity, low background signal, and wide detection range (Wu et al., 2012; Edwards et al., 2015). However, most of the ECL luminophore, including hydrazine compounds

(Bertoncello et al., 2009) and QDs (Li et al., 2016; Chen et al., 2016), were toxic or the synthesis was inefficient, which restricted the application of ECL in biological detection. Therefore, seeking easily synthesized, environmentally friendly, low-toxin or toxin-free ECL luminophore materials was imminent.

Nowadays, low-toxin or toxin-free metal nanoclusters-centric ECL substitutes with outstanding photostability and excellent biocompatibility (Xiao et al., 2015; Feng et al., 2017), such as Au nanoclusters (Au NCs), Ag nanoclusters (Ag NCs) and Cu nanoclusters (Cu NCs) (Fan et al., 2017; Zhou et al., 2017; Song et al., 2015), had become research priorities in actual application of chemical sensing and biosensor detection. Among them, Cu NCs with low-cost and high-efficiency (Zhao et al., 2016), had gained growing popularity in various areas of biosensing and bioimaging. Though considerable synthetic methods for Cu NCs had gained attractive attentions and improvements, most of the methods for preparing stable Cu NCs such as chemosynthesis and solvent reduction, sank into the problems of size control and irreversible aggregation (Miao et al., 2015; Maity et al., 2013; Wang et al., 2014), which were the crucial factors of the luminescent property. Thus, the addition of protecting ligands, mainly involving in DNA (Jia et al., 2012; Rotaru et al., 2010), protein (Goswami et al., 2011), peptides (Yuan et al., 2011) et al, was a significant way to control the aggregation of Cu NCs. Our group had successfully synthesized a BSA-stabilized Cu NCs as ECL probe to construct a “signal-off” ECL system in solution for detecting dopamine (Zhao et al., 2016). However, the strategy failed to immobilize the ECL probe onto the sensing interface, which inhibited the ECL luminous of Cu NCs due to the long electron-transfer path and much energy loss between the luminophor Cu NCs and the sensing interface, limiting the application of Cu NCs in sensitive bioassays. More recently, Wang and co-workers (Wang et al.,

2017) synthesized DNA-stabilized Cu NCs on the electrode by chemical reduction to build an electrochemical aptasensor for miR-21 detection. Although the immobilization of Cu NCs had been settled, the reduction method of Cu NCs is complicated and inefficient. Therefore, it is a great challenge to develop a synthesis method of Cu NCs with high ECL performance, which is simple and able to efficiently immobilize Cu NCs onto the electrode for biosensor construction.

Herein, we have successfully constructed an ultrasensitive biosensor for miR-21 detection by in-situ generation of Cu NCs as ECL luminophore and titanium dioxide (TiO_2) as coreaction accelerator. As shown in Scheme 1A, with the exonuclease III (Exo III) assisting, a small amount of target miR-21 was involved in the cascade signal amplification to output a large number of secondary target (T2). And then, the T2 was introduced to open the hairpin DNA1 strand which was immobilized on the TiO_2@Pt modified sensing interface *via* the Pt-N bond. After that, DNA2 and DNA3 were dropped on the electrode binding the remaining branch of DNA1 to trigger the HCR process for forming plenty AT-rich double-stranded DNA (dsDNA). Finally, after incubating Cu^{2+} on the AT-rich dsDNA (Song et al., 2016), the dsDNA-immobilized Cu NCs probe was in-situ generated on the dsDNA owing to the A-Cu^{2+}-T bond, which could reduce the aggregation-caused self-etching effect of Cu NCs, enhancing the ECL intensity of Cu NCs. What's more, TiO_2 was employed to accelerate the reduction of $S_2O_8^{2-}$, generating the strong oxidizing intermediate radical $SO_4^{\bullet-}$, which could further improve the ECL performance of Cu NCs. The possible luminescent mechanism of the coreaction accelerator system was demonstrated in the supporting information (Fig. S5). As a result, the proposed biosensor showed an outstanding linear relationship in the concentration range of 100 aM to 100 pM with the detection limit of 19.05 aM. Impressively, the biosensor was

successfully applied to the detection of human cervical cancer and human breast cancer cell lysates. This revealed that the ECL biosensor based on Cu NCs showed promising applications in the filed of bioanalysis and clinical diagnosis.

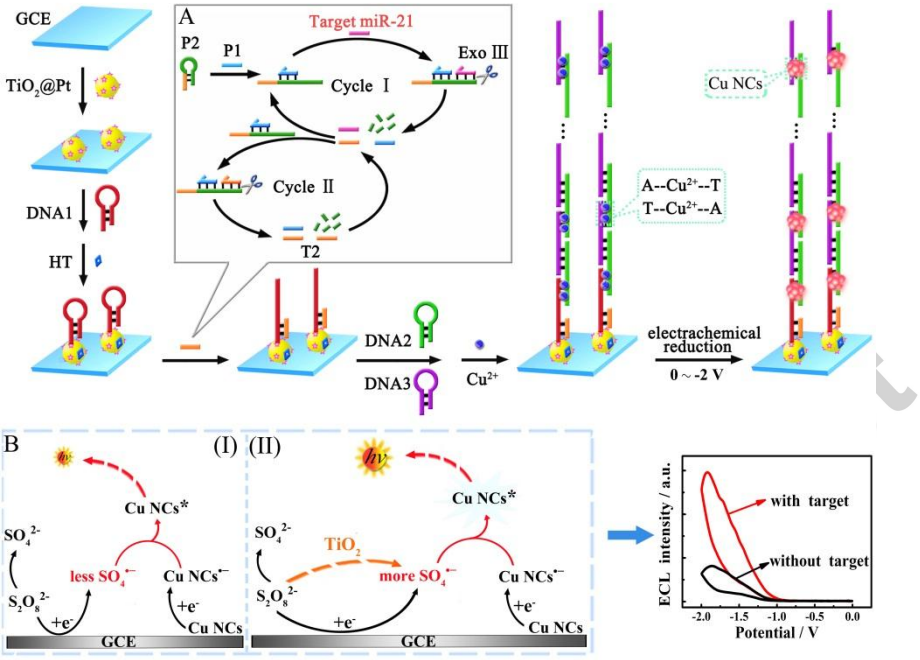

Scheme 1. Schematic diagrams shown the establishment process of biosensor for the ultrasensitive determination of miRNA-21. (A) Exo III-assisted cascade signal amplification process. (B) ECL mechanism of coreaction accelerator system without (I) and with (II) the promotion of TiO_2.

2. Experimental Section

2.1 Preparation of TiO_2@Pt

The synthetic method of TiO_2 was according to the previously published literature (Pan et al., 2014). (The electron microscopic characterization of TiO_2 exhibited in Fig. S1). Firstly, 0.02 g TiO_2 was dissolved in 1 mL of deionized water, and then 500 μL of polyethyleneimine (PEI, 1%) was added. After stirring for 1 h, 500 μL of chloroplatinic acid (H_2PtCl_6, 1 mM) and 100 μL of $NaBH_4$ (1 mM) were added to the above solution, and then keep stirring for 1 h. Finally, the solution was washed twice with deionized water to get rid of the redundant reagents and then the resulting solid was ultrasonic dispersion in 1 mL of deionized water to form TiO_2@Pt

solution.

2.2 Preparation of Secondary target (T2)

The T2 was prepared by reported literature (Gao et al., 2014). First, the P2 (1 μM) was heated to 95 ºC for 5 min to form hairpin structure. And then, the DNA duplex P1-P2 hybrid probe was prepared by mixing 30 μL of P1 (1 μM) and 30 μL of P2 (1 μM) and incubated for 30 min at 25 °C. Second, the P1-P2 hybrid was incubated with 1 μL of Exo III (200 U/μL) which was diluted by Exo III reaction buffer and 30 μL of different concentrations of target miR-21 for 30 min at 37 °C. Finally, the mixture was heated to 70 °C for 5 min to inactivate the Exo III, and the prepared products were reserved at -20 °C for further use. The native PAGE characterization of aforesaid process was revealed in Fig. S3A.

2.3 The Detection of Constructed Biosensor

The step fabrication of the biosensor was shown in Scheme 1. To start with, the bare electrode was polished by aluminum slurry and sonicated with deionized water and ethanol in turn. 5 μL of TiO_2@Pt solution was dropped on the pretreated electrode and dried. Then 5 μL of annealed amino-modified DNA1 (1 μM) was dropped on the electrode surface and incubated for 12 h at 4 °C. Subsequently, the resultant electrode was blocked with 1 mM HT for 30 min. Following that, 10 μL of T2 with different concentrations were incubated on the modified electrode surface for 30 min at room temperature. And then, the annealed 5 μL of DNA2 (1 μM) and 5 μL of DNA3 (1 μM) was dropwise added on the biosensor, incubating for 2 h at room temperature to trigger HCR process for producing numerous AT-rich dsDNA. Ultimately, the biosensor was incubated with 5 μL of $CuSO_4$ solution (100 μM) for 60 min. In the end, the potential from 0 to -2 V with the scan rate of 100 mV/s was applied to the biosensor to realize ECL detection in PBS (0.1 M, pH 7.4) containing 5

mM $K_2S_2O_8$. Completing each step, the modified electrode was rinsed by deionized water to wipe off the physical adsorption. The electrochemical characterization of biosensor construction was shown in Fig. S2 and the native PAGE characterization of HCR process was demonstrated in Fig. S3B.

2.4 Application for Actual Sample Detection

Human breast cancer cells (MCF-7) and human cervical cancer cells (Hela) were chose to examine the actual sample tests. After the cell count treatment, miRNAs were extracted from different amounts of cell samples using column commercial miRNA extraction kits. Finally, the lysates were stored at -20 °C for miR-21 detection. Simultaneously, to verify the analytical performances of the presented biosensor, the quantitative reverse transcription-polymerase chain reaction (qRT-PCR) was employed to detect the actual samples which was used in this study. (The result was shown in Figure S10).

3. Results and discussion

3.1 Structural Characteristics and Optical Characterization of the in-situ Generated Cu NCs

HRTEM were mainly used to study the morphology and size of the in-situ generated Cu NCs. As shown in Fig. 1A, the diameter of Cu NCs were mainly distributed in the range 1−4.5 nm with the average size of 2.5 nm (see the inset of Fig. 1A). Then, the HRTEM image (Fig. 1B) of a sphere revealed that a series of 2D lattice fringes orderly and compactly arrange. The 2D lattice fringes were examined to be 0.209 nm, approaching the (1-11) lattice spacing of the fcc-Cu nanocrystals (Han et al., 2017), which obviously supported its single crystal structure and oriented growth.

Simultaneously, the XPS was employed to investigate the component of Cu NCs. As shown in Fig. 1C, the Cu NCs were composed of C, O, N, and Cu elements. And

then there were two characteristic peaks at 933.30 and 953.35 eV (Fig. 1D), which were owing to $2p_{3/2}$ and $2p_{1/2}$ features of Cu(0) (Wei et al., 2011). Fig. 1E exhibited the UV-Vis absorption spectrum of the DNA and DNA-immobilized Cu NCs. A significant absorption peak could be observed at 260 nm from curve a, which was the characteristic absorption peak of DNA. When Cu NCs were generated in situ, the characteristic absorption peak (curve b) was significantly widened and red shifted, indicating the high affinity of HCR-produced DNA to Cu^{2+}. Furthermore, the ECL emission spectrum (curve b of Fig. 1F) of Cu NCs have a maximum wavelength at about 525 nm. Comparing with PL spectrum (curve a of Fig. 1F), the ECL spectrum showed a longer red shift at the emission peak, which probably owing to the instrument effect and self-absorption of Cu NCs (Hesari et al., 2014). In addition, to verify the luminescence of Cu NCs, the ECL spectrum of the $S_2O_8^{2-}$ solution was exhibited in the Fig. S7.

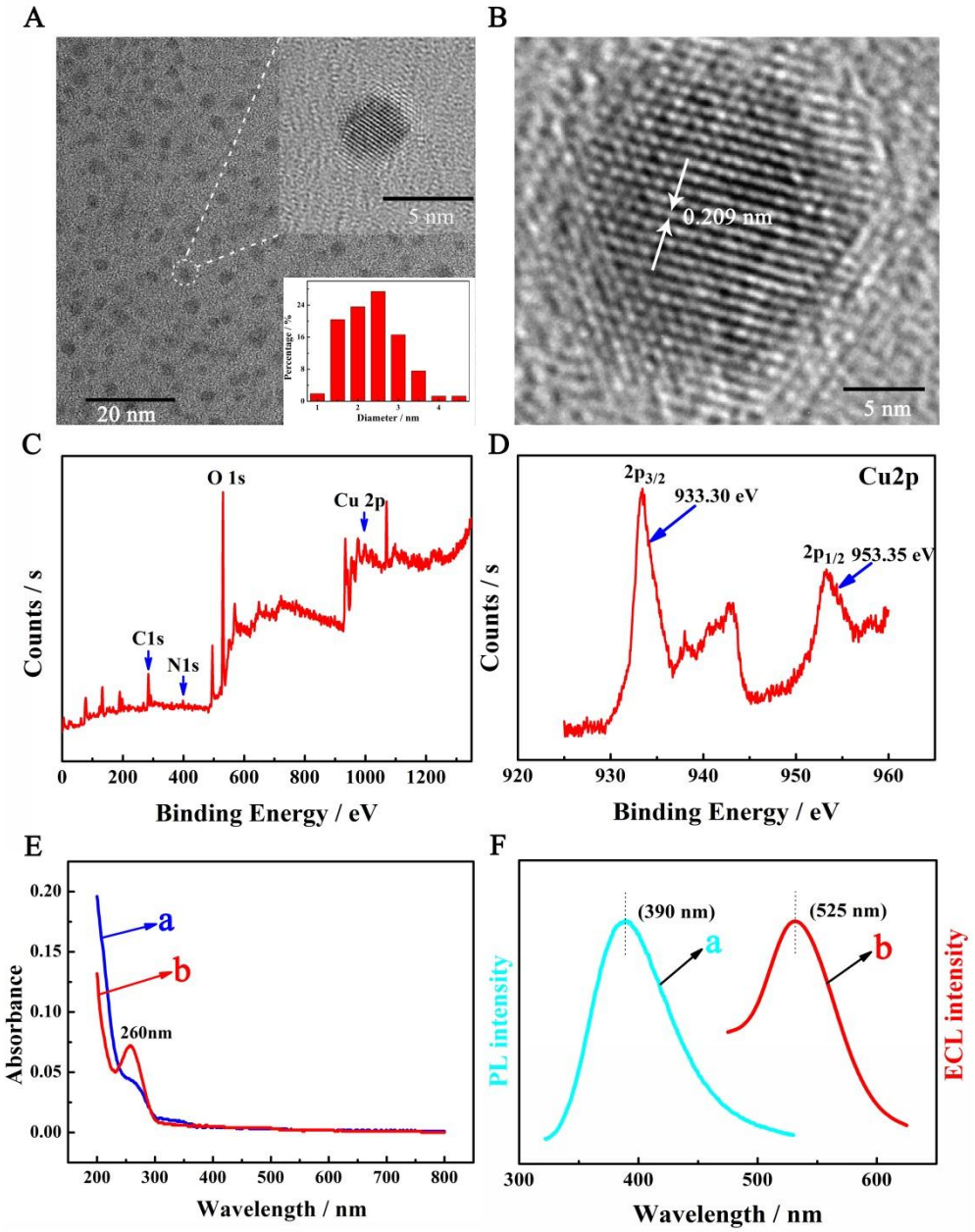

Fig. 1. (A) HRTEM image of the Cu NCs in-situ generated on dsDNA, the two insets exhibited the crystal structure of a single nanocluster and the diameter distribution of Cu NCs, respectively; (B) The crystal lattice of the Cu NCs; XPS spectra shown the full region of (C) DNA-stabilized Cu NCs and (D) Cu 2p region; (E) The UV-vis absorption curves of the DNA (curve a) and DNA-immobilized Cu NCs (curve b); (F) The PL spectrum (curve a) and the ECL spectra (curve b) of the Cu NCs.

3.2 The Analytical Performance of miR-21 Biosensor

The obtained ECL biosensor were quantitatively examined by adding known

concentrations of miR-21 under the optimal conditions (The optimization results of biosensor were presented in Fig. S4). As shown in Fig. 2A, the ECL intensity increased with the incremental concentration of miR-21 from 100 aM to 100 pM and showed an outstanding linear relationship (Fig. 2B). The linear regression equation was: $I = 412.6 \lg c + 8481$ (I represented the intensity of the ECL and c represented the concentration of the target) with the correlation coefficient of $R = 0.9980$. The detection limit of miR-21 is 19.05 aM (S/N = 3, the specific calculation process is shown in supporting information). In addition, we compared the biosensor with other methods for miR-21 detection, and the results were shown in Table S2, proving that the present biosensor had a low detection limit and even better sensitivity.

The stability was a key factor in judging the performance of biosensors. As shown in Fig. 2C, with the increase of miRNA-21 concentrations, the scanning curves were comparatively stable at each concentration for three consecutive cycles, suggesting good stability for the proposed biosensor. Simultaneously, miR-155 (1 nM), miR-141 (1 nM) and miR-199A (1 nM) were selected as the interference substances to investigate the selectivity of the miR-21 biosensor. As shown in Fig. 2D, using miR-155 (1 nM), miR-141 (1 nM) and miR-199A (1 nM) replaced miRNA-21 (10 pM), respectively, for exploring contrast experiments. As expected, there were did not shown any distinct increase between the interfering agents and the blank, while the pure miRNA-21 and the mixture containing miRNA-21 (10 pM) expressed no remarkable difference. These results proved that the proposed biosensor exhibited excellent selectivity.

In order to research the practicability of our method, we investigated the expression of miRNA-21 in cell lysates, the results was shown in Fig. S9, which was comparable to previous reports (Liao et al., 2014; Yin et al., 2012). Simultaneously to

further estimate the reproducibility of the proposed biosensor, we explored the intra- and inter-assays. As shown in Figure S7, the values of relative standard deviation (RSD) in intra- and inter-assays were all below 5%, suggesting the outstanding reproducibility of the ECL biosensor. To verify the analytical performances of the proposed biosensor, the quantitative reverse transcription-polymerase chain reaction (qRT-PCR) was employed to detect the actual samples which was used in this study, the results was shown in Fig. S10.

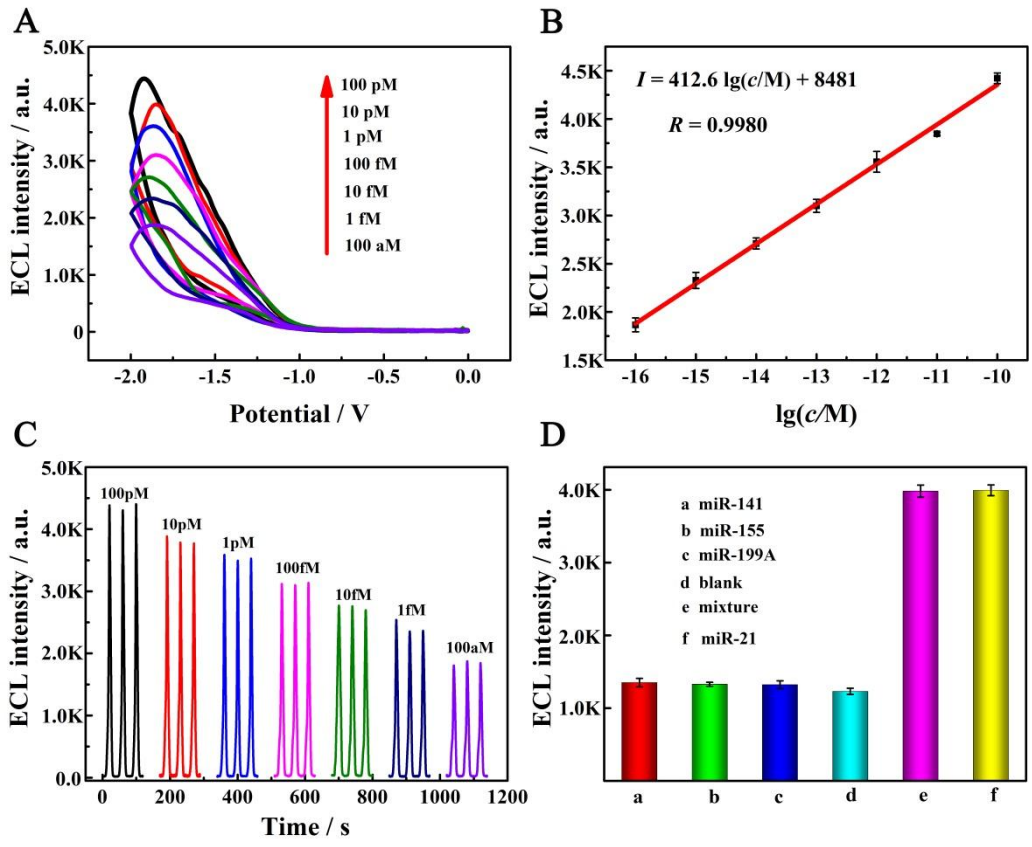

Fig. 2. The relationship between the ECL signal of biosensor and the miR-21 concentration. (A) The ECL intensity-voltage curves of the biosensor under different miR-21 concentrations. (B) Linearity curve for biosensors for miR-21 assays. (C) The ECL stability of biosensor from 100 pM to 100 aM of miR-21. (D) The selectivity of ECL biosensor: (a) 1 nM of miR-141, (b) 1 nM of miR-155, (c) 1 nM of miR-199A, (d) blank, (e) a mixture (containing miR-141 (1 nM), miR-155 (1 nM), miR-199A (1 nM) and 10 pM miR-21 (10 pM)), (f) miR-21 (10 pM).

4. Conclusions

In summary, we proposed an ultrasensitive ECL biosensor based on in-situ generation of copper nanoclusters as luminophore and TiO_2 as coreaction accelerator for miR-21 detection and the proposed strategy has the following two new point. First, a novel, simple and fast synthesis method was proposed to generate the high ECL performance of Cu NCs on the electrode through in-situ electrochemical reduction. Second, TiO_2 was employed not just acted as the immobilizer of dsDNA-stabilized Cu NCs, more than acted as the coreaction accelerator to accelerate the reduction of the $S_2O_8^{2-}$ for significantly enhancing the ECL efficiency of Cu NCs. Furthermore, the coreaction accelerator system provided a substantive progress for Cu NCs-based ECL biosensor in the anticipated developing field.

Acknowledgements

This work was financially supported by the National Natural Science Foundation (NNSF) of China (Grants 21675130, 21575116 and 51473136) and the Fundamental Research Funds for the Central Universities (Grant XDJK2017A001), China.

oligonucleotides sequences used in this work.

Supporting information

Supporting file includes the oligonucleotides sequences used in this work (Table. S1). Comparison of existing miR-21 detection methods (Table. S2). SEM image of TiO_2 (Fig. S1). Electrochemical characterization of biosensor construction (Fig. S2). Native PAGE characterization of the signal amplification strategy (Fig. S3). Optimization conditions of ECL biosensor (Fig. S4). Possible ECL emitting mechanisms (Fig. S5). The reduction time of Cu^{2+} (Fig. S6). The ECL spectrum of the Cu NCs and $S_2O_8^{2-}/O_2$ ECL system (Fig. S7). Reproducibility of the miRNA biosensor (Fig. S8). The

practical application of biosensor (Fig. S9).

References

Bertoncello, P., Forster, R.J., 2009. Biosens. Bioelectron. 24, 3191–3200.

Chen, A.Y., Ma, S.Y., Zhuo, Y., Chai, Y.Q., Yuan, R., 2016. Anal. Chem. 88, 3203–3210.

Chen, J., Kong, Y.F., Wang, W., Fang, H.W., Wo, Y., Zhou, D.J., Wu, Z.Y., Li, Y.X., Chen, S.Y., 2016. Chem. Commun. 52, 4025−4028.

Edwards, M., McConnell, P., Schafer, D.A., Cooper, J.A., 2015. Nat. Commun. 6, 8415.

Fan, Y., Tan, X.G., Ou, X., Chen, S.H., Wei, S.P., 2017. Biosens. Bioelectron. 87, 802−806.

Feng, L.Y., Wu, L., Xing, F.F., Hu, L.Z., Ren, J.S., Qu, X.G., 2017. Biosens. Bioelectron. 98, 378−385.

Gao, Y., Li, B.X., 2014. Anal. Chem. 86, 8881-8887.

Goswami, N., Giri, A., Bootharaju, M.S., Xavier, P.L., Pradeep, T., Pal, S.K., 2011. Anal. Chem. 83, 9676−9680.

Han, G., Xie, Z.J., Li, Z.Y., Lei, B., Shang, C.J., Misra, R.D.K., 2017. Mater Design 135, 92-101.

Hesari, M., Workentin, M.S., Ding, Z.F., 2014. ACS Nano 8, 8543−8553.

Jia, X.F., Li, J., Han, L., Ren, J.T., Yang, X. Wang, E.K., 2012. ACS Nano 6, 3311−3317.

Lei, Y.M., Zhao, M., Wang, A., Yu, Y.Q., Chai, Y.Q., Yuan., Zhuo, Y., 2016. Chem. Eur. J. 22, 8207−8214.

Li, M.X., Zhao, W., Qian, G.S., Feng, Q.M., Xu, J.J., Chen, H.Y., 2016. Chem.

Commun. 52, 14230–14233.

Liao, Y.H., Huang, R., Ma, Z.K., Wu, Y.X., Zhou, X.M., Xing, D., 2014. Anal. Chem. 86, 4596−4604.

Lu, S.S., Wang, S., Zhao, J.H., Sun, J., Yang, X.R., 2017. Anal. Chem. 89, 8429–8436.

Maity, P., Yamazoe, S., Tsukuda, T., 2013. ACS Catal. 3, 182−185.

Miao, H., Zhong, D., Zhou, Z.N., Yang, X.M., 2015. Nanoscale 7, 19066−19072.

Pan, J.H., Wang, X.Z., Huang, Q.Z., Shen, C., Koh, Z.Y., Wang, Q., Engel, A., Bahnemann, D.W., 2014. Adv. Funct. Mater. 24, 95−104.

Rotaru, A., Dutta, S., Jentzsch, E., Gothelf, K., Mokhir, A., 2010. Angew. Chem. 49, 5665−5667.

Song, Q.W., Shi, Y., He, D.C., Xu, S.H. Ouyang, J., 2015. Chem. Eur. J. 21, 2417-2422.

Wang, C., Wang, C., Xu, X.L., Cheng, H., Lin, Q., Zhang, C., 2014. Nanoscale 6, 1775−1781.

Wang, Y.J., Zhang, X.Y., Zhao, L., Bao, T., Wen, W., Zhang, X.H., Wang, S.F., 2017. Biosens. Bioelectron. 98, 386−391.

Wei, W.T., Lu, Y.Z., Chen, W., Chen, S.W., 2011. J. Am. Chem. Soc. 133, 2060−2063.

Wu, L., Wang, J.S., Feng, L.Y., Ren, J.S., Wei, W.L., Qu, X.G., 2012. Adv. Mater. 24, 2447–2452.

Wu, P., Hou, X.D., Xu, J.J., Chen, H.Y., 2016. Nanoscale 8, 8427–8442.

Xiao, F.X., Zeng, Z.P., Liu, B., 2015. J. Am. Chem. Soc. 137, 10735−10744.

Yuan, X., Luo, Z.T., Zhang, Q.B., Zhang, X.H., Zheng, Y.G., Lee, J.Y., Xie, J.P., 2011. ACS Nano 5, 8800−8808.

Yin, B.C., Liu, Y.Q., Ye, B.C., 2012. J. Am. Chem. Soc. 134, 5064−5067.

Zaleska, K., Przybyła, A., Kulcenty, K., Wichtowski, M., Mackiewicz, A., Suchorska, W., Murawa, D., 2017. Oncology Letters 14, 4029-4036.

Zhao, M., Chen, A.Y., Huang, D., Zhuo, Y., Chai, Y.Q., Yuan, R., 2016. Anal. Chem. 88, 11527−11532.

Zhou, Y., Chen, M.X., Zhuo, Y., Chai, Y.Q., Yuan, R., 2017. Anal. Chem. 89, 6787−6793.

Highlights

- A novel, simple and fast synthesis method was proposed to generate the high ECL performance of Cu NCs through in situ electrochemical reduction.
- $S_2O_8^{2-}$ as coreaction and TiO_2 as coreaction accelerator were employed to construct a Cu NCs-based ECL biosensor for miR-21 detection.
- The ECL biosensor exhibited high selectivity, excellent stability and low detection limit of 19.05 aM for miR-21.